Concerning pion structure using continuum Schwinger function methods

Minghui Ding[12]

[1] School of Physics, Nanjing University, Nanjing, Jiangsu 210093, China
[2] Institute for Nonperturbative Physics, Nanjing University, Nanjing, Jiangsu 210093, China

Light-Cone 2024: Hadron Physics in the EIC era
Institute of Modern Physics, Chinese Academy of Sciences, Huizhou, Guangdong, China

November 27, 2024

1 Introduction

2 Form factors

3 1D picture of how quarks move within pion

4 A multidimensional view of pion structure

Emergence

- Aristotle, Metaphysics, Book VIII (Eta) 1045a 8-10:
  "... the totality is not, as it were, a mere heap, but the whole is something besides the parts ...", i.e., **the whole is more than the sum of the parts**.

Proton mass

- Proton mass: 938 MeV,
  mass scale charactering all visible matter.
- Its components:
  up (u) and down (d) quarks: $m_u + m_u + m_d \approx 9$ MeV
  – generated by Higgs Mechanism in the Standard Model.
- Proton mass is 100-times greater than sum of masses of its valence constituents.

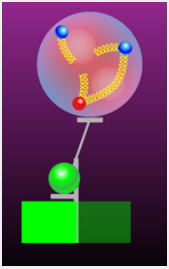

Proton mass is an emergent feature of QCD, the same as pion, emergence of hadron mass (EHM) must provide a link between theory and Nature.

Naive picture:
up quark + down antiquark:

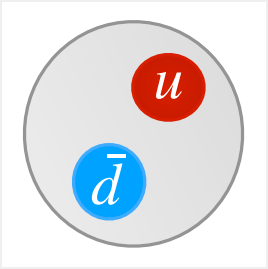

Realistic picture:
up quark + down antiquark + sea quarks + gluons

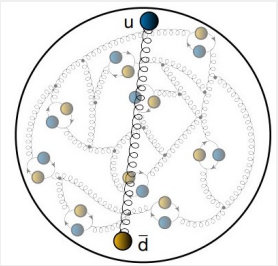

- Mass: ~ 140 MeV; the lightest hadron; spin 0; P parity $-$; pseudoscalar meson.
- Nambu-Goldstone bosons of spontaneously broken chiral symmetry.

Pion does not fit naturally into the mass pattern typical of constituent quark model:

Maris, Roberts, Tandy, Phys. Lett. B 420 (1998) 267-273.

$$f_\pi m_\pi^2 = 2 m_u \rho_\pi \tag{1}$$

f_π, leptonic decay constant; m_π, pion mass; m_u, current quark mass; ρ_π, pseudoscalar projection of the pion wave function onto the origin in configuration space.

- Gell-Mann-Oakes-Renner (GMOR) relation
- Pion mass m_π vanishes in the absence of current quark mass m_u - Nambu-Goldstone boson of chiral symmetry breaking (when current quark mass is zero, QCD Lagrangian possesses a chiral symmetry).
- Mass square of pion rises linearly with the current quark mass, $m_\pi^2 \propto m_u$, whereas in constituent quark model $m_{\text{meson}} \propto m_{\text{quark}}$.

Axial-vector Ward-Takahashi identity in chiral limit: $\mathcal{M}^{ab} = 0$; anomaly: $\mathcal{A}^a(k;P) = 0$.

$$P_\mu \Gamma^a_{5\mu}(k;P) = \mathcal{S}^{-1}(k_+) i\gamma_5 \mathcal{F}^a + i\gamma_5 \mathcal{F}^a \mathcal{S}^{-1}(k_-) \tag{2}$$

Quark propagator: $S^{-1}(k) = i\gamma\cdot k A(k^2) + B(k^2)$, right hand side:

$$\lim_{P^2\to 0} R = i\gamma_5 B(k^2)\,, \tag{3}$$

Massless pion pole in axial vector vertex: $\Gamma_{5\mu}(k,P) \xrightarrow{P^2=-m_\pi^2} \frac{f_\pi P_\mu}{P^2+m_\pi^2}\Gamma_\pi(k;P)$, left hand side:

$$\lim_{P^2\to 0} L = i\gamma_5 f_\pi E_\pi(k;P=0)\,, \tag{4}$$

Compare Eq.(3) and Eq.(4)

$$f_\pi E_\pi(k;P=0) = B(k^2)\,. \tag{5}$$

Pion's Goldberger-Treiman relation: Maris, Roberts, Tandy, Phys. Lett. B 420 (1998) 267-273.

$$f_\pi E_\pi(k; P=0) = B(k^2) \tag{6}$$

Pion's Bethe-Salpeter amplitude, solution of the Bethe-Salpeter equation

$$\Gamma_\pi(k; P) = \gamma_5[iE_\pi(k; P) + \gamma\cdot P F(k; P) + \gamma\cdot k k\cdot P G(k; P) + \sigma_{\mu\nu} k_\mu P_\nu H(k; P)] \tag{7}$$

Dressed-quark propagator

$$S^{-1}(k) = i\gamma\cdot k A(k^2) + B(k^2) \tag{8}$$

Dynamical chiral symmetry breaking (DCSB) $\Leftrightarrow$ Goldstone theorem

- Pion exists if, and only if, mass is dynamically generated
- Algebraically explain why pion is massless in the chiral limit
- Two body problem is solved, almost completely, once solution of one body problem is known

Quark propagator:

$$S(k;\zeta) = \frac{1}{i\gamma\cdot k A(k^2;\zeta) + B(k^2;\zeta)} = \frac{Z(k^2;\zeta)}{i\gamma\cdot k + M(k^2)} \tag{9}$$

- Massless partonic quarks acquire a momentum dependent mass function which is large at infrared momenta.
- This mass scale is responsible for all hadron masses.
- Properties of the nearly massless pion are the clearest window onto emergence of hadron mass (EHM) in the Standard Model.

Roberts, Richards, Horn, Chang, Prog. Part. Nucl. Phys. 120 (2021) 103883.

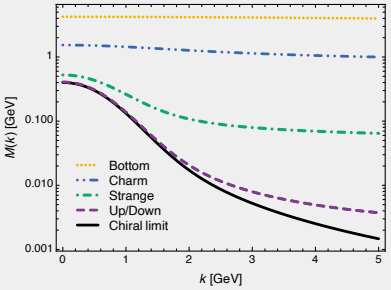

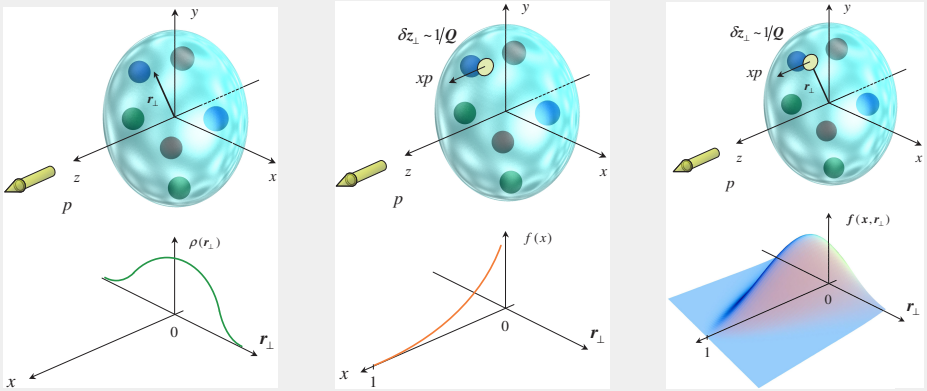

Probabilistic interpretation of (1) Form Factor, (2) Parton distribution function (PDF) and (3) Generalized parton distribution (GPD) at $\eta = 0$ in the infinite momentum frame $p_z \to \infty$.

Form factor: the closest thing we have to a snapshot, the size, shape and makeup of pion

- Electromagnetic form factor
- Two-photon transition form factor
- Gravitational form factor

1D picture of how quarks move within pion

- Parton distribution amplitude
- Parton distribution function (PDF)

A multidimensional view of pion structure

- Transverse momentum dependent distribution function (TMD)
- Generalized parton distribution (GPD)

1 Introduction

2 Form factors

3 1D picture of how quarks move within pion

4 A multidimensional view of pion structure

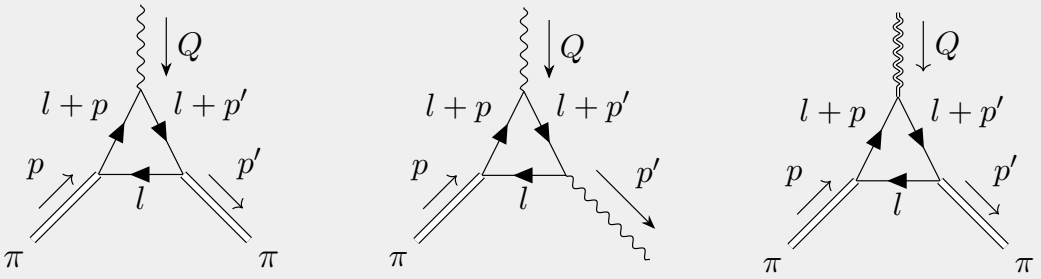

(1) electromagnetic form factor; (2) two-photon transition form factor; (3) gravitational form factor.

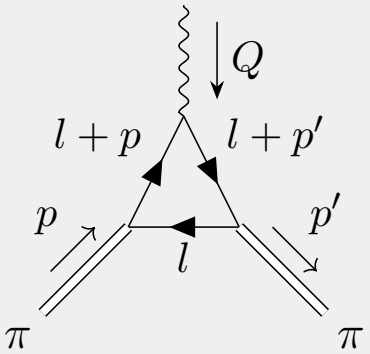

Figure 1: Feynman diagram for $\pi^+(p) \to \pi^+(p')$ elastic electromagnetic form factor $F_\pi(Q^2)$.

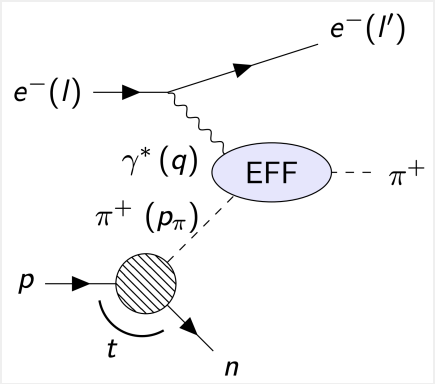

Figure 2: No free pion target - use "virtual pion cloud" of the proton.

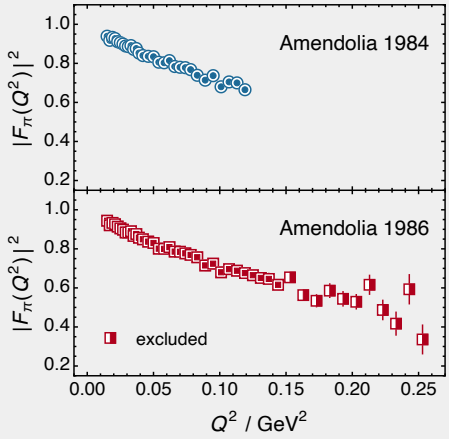

Figure 3: Data collected at CERN by the NA7 Collaboration. Cui, Binosi, Roberts, Schmidt, Phys. Lett. B 822 (2021) 136631.

Electric radius-squared is obtained from the slope of the form factor at $Q^2 = 0$,

$$r_\pi^2 = -\frac{6}{F_\pi(0)} \frac{d}{dQ^2} F_\pi(Q^2)\Big|_{Q^2=0}, \tag{10}$$

and $r_\pi \approx 0.640(7)$ fm.

Large-Q^2 behaviour of pion electromagnetic form factor is predicted by perturbative QCD as:

$$\exists Q_0 > \Lambda_{\rm QCD}\,,$$
$$Q^2 F_\pi(Q^2) \overset{Q^2>Q_0^2}{\approx} 16\pi\alpha_s(Q^2) f_\pi^2 w_\varphi^2(Q^2), \quad (11)$$

where: f_π is the decay constant; $\alpha_s(Q^2)$ is the running-coupling, and $w_\varphi(Q^2)$ is determined by parton distribution amplitude (PDA).

- What is the value of Q_0 for which scaling violations become apparent?
- $Q^2 F_P(Q^2)$ maximum lies in the neighbourhood $Q^2 \simeq 5\,\text{GeV}^2$.
- Thereafter, scaling violation apparent, $Q^2 F_P(Q^2)$ falls steadily toward zero.

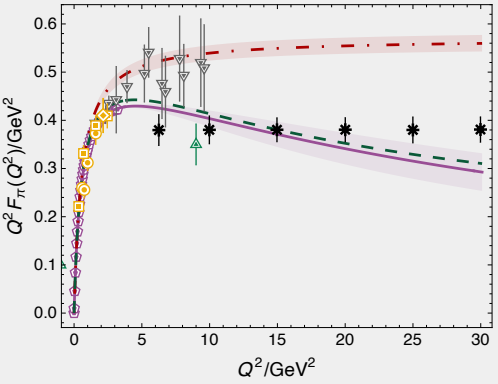

Figure 4: $Q^2 F_\pi(Q^2)$. Precision of lQCD (grey points) is insufficient to distinguish between VMD estimate and CSM prediction. Yao, Binosi, Roberts, Phys.Lett.B 855 (2024) 138823.

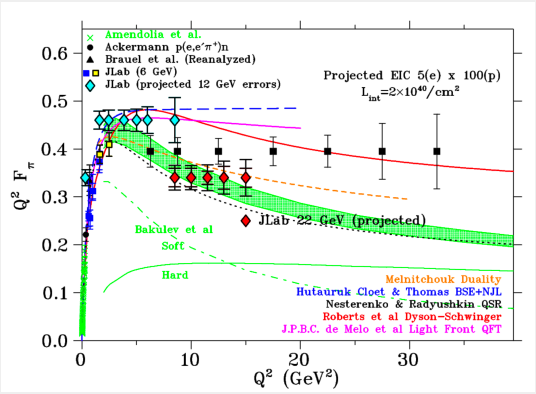

Figure 5: $Q^2F_\pi(Q^2)$, figure is taken from JLab 22 GeV white paper. Eur.Phys.J.A 60 (2024) 9, 173

- Existing data (blue, black, yellow, green) and projected uncertainties for future data on the pion form factor from JLab (12 GeV: cyan; 22 GeV: red) and EIC (black), in comparison to a variety of hadronic structure models. Dyson-Schwinger Equation: Chang, Clot, Roberts, Schmidt, Tandy, Phys. Rev. Lett. 111 (2013) 14, 141802. Chen, Ding, Chang, Roberts, Phys. Rev. D 98 (2018) 9, 091505. Yao, Binosi, Roberts, Phys.Lett.B 855 (2024) 138823.

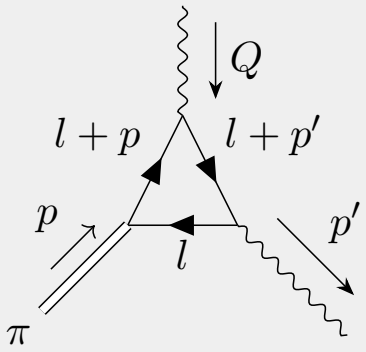

Figure 6: Feynman diagram for $\gamma\gamma^* \to \pi^0$, neutral pion electromagnetic transition form factor $G_\pi(Q^2)$.

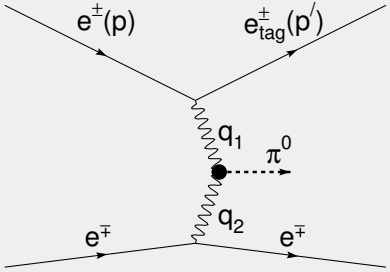

Figure 7: Single-tagged mode: $q_1^2 \neq 0, q_2^2 \approx 0$.

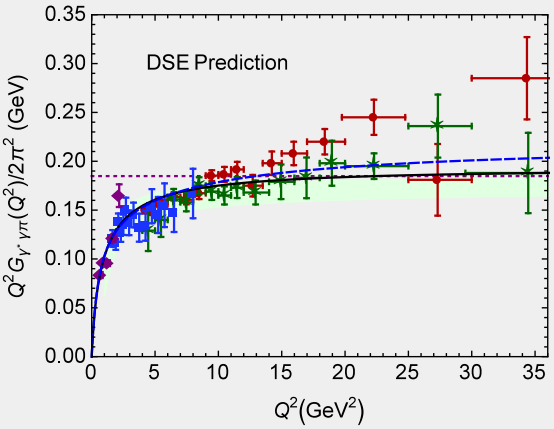

Figure 8: Data: CELLO - diamonds (purple); CLEO - squares (blue); BaBar - circles (red); Belle - stars (green). CSMs results favor the Belle data, The situation may be clarified by upcoming data from BelleII. Raya, Chang, Bashir, Cobos-Martinez, Gutierrez-Guerrero, Roberts, Tandy, Phys. Rev. D 93 (2016) 7, 074017. Eichmann, Fischer, Weil, Williams, Phys. Lett. B 774 (2017) 425-429.

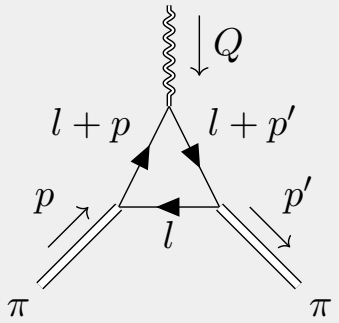

Figure 9: Feynman diagram for pion gravitational form factors.

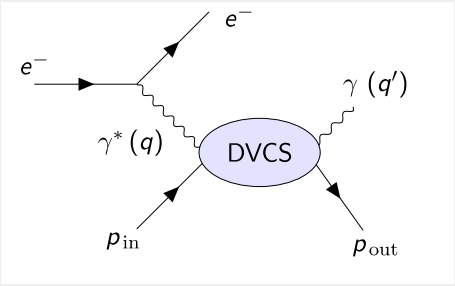

Figure 10: Deep Virtual Compton Scattering (DVCS).

No direct way to measure the hadron gravitational form factor, but it may be probed indirectly in DVCS, through its connection with generalized parton distributions (GPDs):
$\int_{-1}^{1} dx\, x\, H^q(x,\xi,Q^2) = A^q(Q^2) + \xi^2 D^q(Q^2)$.

The gravitational form factors of pion can be extracted from its matrix elements of the energy-momentum tensor (EMT)

$$\langle p'|T^{\mu\nu}|p\rangle = M^{\pi}_{\mu\nu}(Q^2) = 2P_\mu P_\nu A(Q^2) + \frac{1}{2}\left(Q_\mu Q_\nu - Q^2\delta_{\mu\nu}\right) D(Q^2) + 2m_\pi^2 \delta_{\mu\nu}\bar{c}(Q^2)\,,$$

D-term: form factor at $Q^2 = 0$, i.e., $D \equiv D(0)$.

- The last global unknown global property, just like electric charge, magnetic moment, mass, spin etc. Polyakov, Schweitzer, Int.J.Mod.Phys.A 33 (2018) 26, 1830025.
- Always negative, Goldstone boson in the soft-pion limit: $D = -1$.

Gravitational form factor $A(Q^2)$ and $D(Q^2)$: define the mass radius and pressure distribution radius

$$r_A^2 = -\frac{6}{A_\pi(0)}\,\frac{d}{dQ^2}A_\pi(Q^2)\bigg|_{Q^2=0}, \qquad r_D^2 = -\frac{6}{D_\pi(0)}\,\frac{d}{dQ^2}D_\pi(Q^2)\bigg|_{Q^2=0}. \tag{12}$$

Recent analysis yields $r_A = 0.51(2)$ fm, and $r_D = 0.80(4)$ fm, recall charge radius $r_F \approx 0.640(7)$ fm. The mass radius is predicted to be somewhat smaller than its charge radius. Xu et al, Chin. Phys. Lett. 40 (2023) 4, 041201. Xu et al, Eur. Phys. J. C 84 (2024) 2, 191.

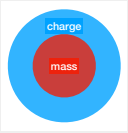

1 Introduction

2 Form factors

3 1D picture of how quarks move within pion

4 A multidimensional view of pion structure

Large-Q^2 behaviour of pion electromagnetic form factor is predicted by perturbative QCD (pQCD) analyses as:

$$\exists Q_0 > \Lambda_{\rm QCD} \mid Q^2 F_\pi(Q^2) \overset{Q^2>Q_0^2}{\approx} 16\pi\alpha_s(Q^2) f_\pi^2 w_\varphi^2(Q^2), \tag{13}$$

where: f_π is the pion's leptonic decay constant; $\alpha_s(Q^2)$ is the strong running-coupling, and

$$w_\varphi(Q^2) = \frac{1}{3}\int_0^1 dx\, \frac{1}{x}\varphi_\pi(x;Q^2)\,, \tag{14}$$

where $\varphi_\pi(x;Q^2)$ is the pion's valence-quark leading-twist parton distribution amplitude (PDA).
On the domain $\Lambda_{\rm QCD}^2/Q^2 \simeq 0$,

$$\varphi_\pi(x;Q^2) \overset{\Lambda_{\rm QCD}^2/Q^2\simeq 0}{\approx} \varphi_\pi^{\rm cl}(x) = 6x(1-x)\,; \tag{15}$$

and hence

$$Q^2 F_\pi(Q^2) \overset{\Lambda_{\rm QCD}^2/Q^2\simeq 0}{\approx} 16\pi\alpha_s(Q^2) f_\pi^2\,. \tag{16}$$

Dyson-Schwinger Equation: Chang, Cloet, Cobos-Martinez, Roberts, Schmidt, Tandy, Phys. Rev. Lett. 110 (2013) 13, 132001.

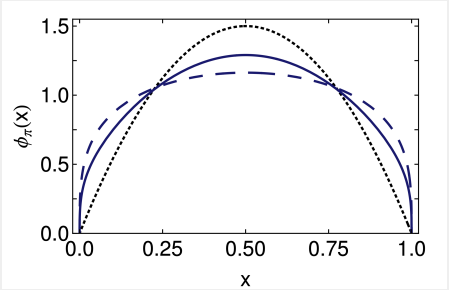

Figure 11: Curves: solid, DCSB-improved kernel (DB); dashed, rainbow ladder (RL); and dotted, asymptotic distribution.

Lattice QCD with Large Momentum Effective Theory (LaMET) approach:

Zhang, Honkala, Lin, Chen, Phys. Rev. D 102, 094519 (2020).

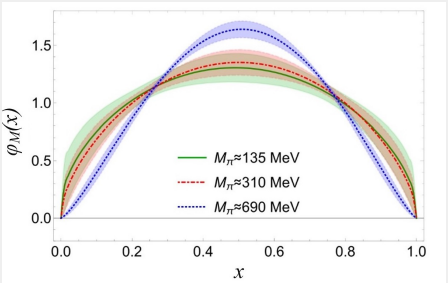

Figure 12: Pion distribution amplitude dependence on pion mass. The lighter mesons have a broader distribution.

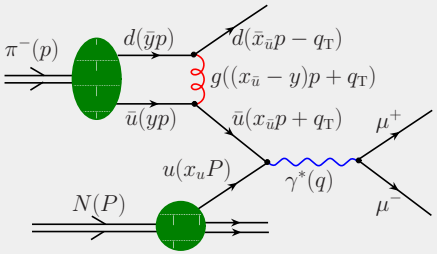

Figure 13: Graphical representation of the Drell-Yan process $\pi^- N \to \mu^+\mu^- X$.
Xing, Ding, Cui, Pimikov, Roberts, Schmidt, Phys.Lett.B 849 (2024) 138462.

- Using a reaction model, the differential cross-section is

$$\frac{d^5\sigma(\pi^- N \to \mu^+\mu^- X)}{dQ^2 dQ_T^2 dx_L d\cos\theta d\phi} \propto N(\tilde{x}, \rho) \times \left[1 + \lambda\cos^2\theta + \mu \sin 2\theta \cos\phi + \tfrac{1}{2}\nu \sin^2\theta \cos 2\phi + \bar{\mu} \sin 2\theta \sin\phi + \tfrac{1}{2}\bar{\nu} \sin^2\theta \sin 2\phi\right],$$

  the last line contributes when nucleon target is longitudinally polarized.
- Angular distribution parameters λ, μ, ν (unpolarized target) and $\bar{\mu}, \bar{\nu}$ (longitudinally polarized proton) are sensitive to pointwise form of pion PDA.
- The precision of extant data is insufficient for use in charting pion PDA.

Synergy

- Experiments:
  - In the past: awarded a high priority – Led to
    (i) the discovery of quarks;
    (ii) Nobel prizes for the experiment leaders;
    (iii) the development of quantum chromodynamics (QCD)
  - Ongoing and in plan:
    Proposals at Jefferson Lab 22 GeV;
    CERN: COMPASS++/AMBER;
    Electron Ion Collider (EIC) in USA;
    Electron-ion collider in China (EicC).
- Global fits:
  Inferred from data, results viewed as benchmarks
- Continuum methods and Lattice QCD:
  Historically, yielded only low-order Mellin moments. Pointwise behavior was not accessible.

- Concept (I): at a hadron scale ζ_H, dressed valence-quarks carry all the pion's light-front momentum and the glue and sea distributions vanish.

  Ding, Raya, Binosi, Chang, Roberts, Schmidt, Phys. Rev. D 101 (2020) 5, 054014

$$u^\pi(1-x,\zeta_H) = u^\pi(x,\zeta_H) \tag{17}$$

- Numerically solve the bound-state equations to calculate valence distribution at hadron scale.
- Concept (II): a proposition, there exists an effective charge, $\alpha_{1\ell}(k^2)$, that, when used to integrate the one-loop pQCD Dokshitzer-Gribov-Lipatov-Altarelli-Parisi (DGLAP) equations, defines an evolution scheme for parton PDFs that is all-orders exact.

  Raya, Cui, Chang, Morgado, Roberts, Rodríguez-Quintero, Chin. Phys. C 46 (2022) 1, 013105.

$$\frac{\langle x^n q^M\rangle_\zeta}{\langle x^n q^M\rangle_{\zeta_H}} = \exp\left[\frac{\gamma_0^n}{4\pi}\int_{\ln\zeta^2}^{\ln\zeta_H^2} d(\ln k^2)\,\hat{\alpha}(\ln k^2)\right] \tag{18}$$

- Evolve parton distribution function from hadron scale ζ_H to any other scale ζ.

Leading-twist valence quark PDF in the operator representation:

$$q(x) = \frac{1}{4\pi}\int dz^- e^{-ixP^+z^-}\langle P|\bar{\psi}(z^-)U^{-\dagger}_{(+\infty;z)}\gamma^+ U^-_{(+\infty;0)}\psi(0)|P\rangle\,, \tag{19}$$

Light-cone gauge: $n\cdot A = 0$, Wilson line $U^{-\dagger}_{(+\infty;z)} = U^-_{(+\infty;0)} = 1$. In the parton model,

$$q(x) = \int \frac{d^4k}{(2\pi)^4}\delta\left(n{\cdot}k - xn{\cdot}P\right)\,\mathrm{Tr}\left[i\gamma{\cdot}n\,G(k,P)\right]\,. \tag{20}$$

Pion PDF at hadron scale:

$$q^\pi(x;\zeta_H) = N_c\mathrm{tr}\int_{dk}\delta^x_n(k_\eta)\;n\cdot\partial_{k_\eta}\left[\Gamma_\pi(k_\eta,-P;\zeta_H)S(k_\eta)\right]\Gamma_\pi(k_{\bar{\eta}},P)\,S(k_{\bar{\eta}})\,, \tag{21}$$

$S(k)$, quark propagator; $\Gamma_\pi(k,P;\zeta_H)$, pion Bethe-Salpeter amplitude.

- Green function of different order couples to each other - truncation
- Some equations are extremely complicated - modeling
- Non-perturbative approach

Eichmann, arXiv:0909.0703.

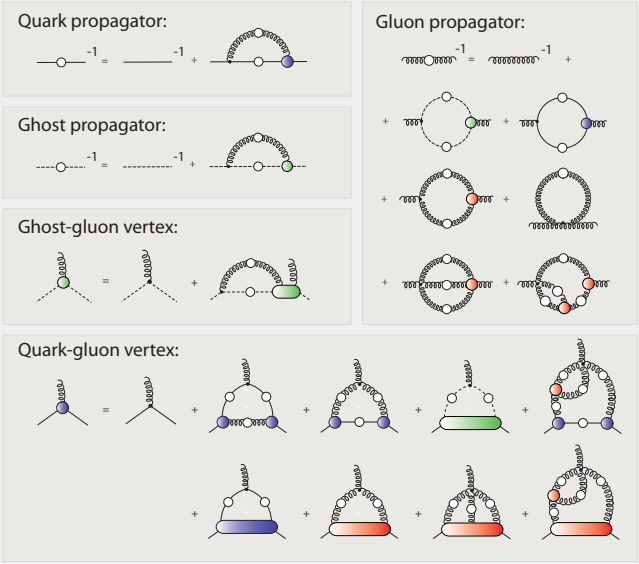

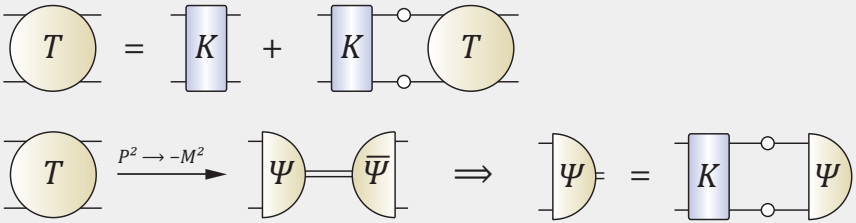

- The two-particle propagator can be expressed in terms of pole contributions, and the residue is the Bethe-Salpeter wave function.
- Bethe-Salpeter Equation.

- Solid navy curve:
  $q^{\pi}(x;\zeta_H) = 213.32\,x^2(1-x)^2[1 - 2.9342\sqrt{x(1-x)} + 2.2911\,x(1-x)]$,
- Long-dashed green curve:
  $q^{\pi}_{\tilde{\varphi}^2}(x;\zeta_H) = 301.66x^2(1-x)^2[1 - 2.3273\sqrt{x(1-x)} + 1.7889\,x(1-x)]^2$.
- Dotted black curve: scale free result
  $q_{\rm sf}(x) = 30x^2(1-x)^2$.
- A broad function, induced by dynamical chiral symmetry breaking, and emergence of hadron mass (EHM).
- Large x behaviour:
  $q^{\pi}(x;\zeta_H) \sim (1-x)^2$.

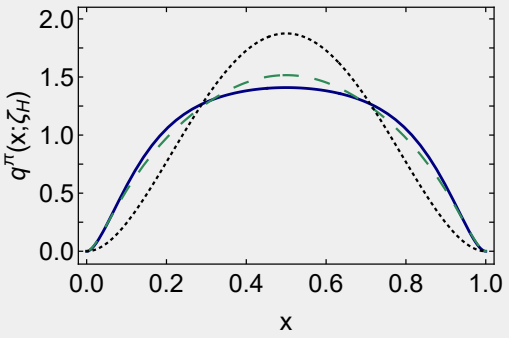

- Existing Lattice QCD calculations of low-order moments and phenomenological fits to pion parton distributions are quoted at $\zeta_2 = 2$ GeV, evolving $q^\pi(x;\zeta_H) \to q^\pi(x;\zeta_2)$.
- Experiment takes the average scale $\zeta_5 = 5.2$ GeV, evolving $q^\pi(x;\zeta_H) \to q^\pi(x;\zeta_5)$.
- Proposition: There exists an effective charge, $\alpha_{1\ell}(k^2)$, that, when used to integrate the one-loop pQCD DGLAP equations, defines an evolution scheme for parton PDFs that is all-orders exact. $\alpha_{1\ell}(k^2)$ need not be unique (We use process-independent charge here).

Valence quark distribution PDF Mellin moments: Raya, Cui, Chang, Morgado, Roberts, Rodríguez-Quintero, Chin. Phys. C 46 (2022) 1, 013105.

$$\frac{\langle x^n q^M\rangle_\zeta}{\langle x^n q^M\rangle_{\zeta_H}} = \exp\left[\frac{\gamma_0^n}{4\pi}\int_{\ln\zeta^2}^{\ln\zeta_H^2} d(\ln k^2)\,\hat\alpha(\ln k^2)\right], \tag{22}$$

Sea quark and gluon PDF Mellin moments: (generated by valence PDF at hadron scale)

$$\begin{pmatrix}\langle x^n\rangle_\Sigma^\zeta\\ \langle x^n\rangle_g^\zeta\end{pmatrix} = \begin{pmatrix}\alpha_+^n S_-^n + \alpha_-^n S_+^n\\ \beta_{g\Sigma}^n\left(S_-^n - S_+^n\right)\end{pmatrix}\begin{pmatrix}\langle x^n\rangle_\Sigma^{\zeta_H}\\ 0\end{pmatrix}. \tag{23}$$

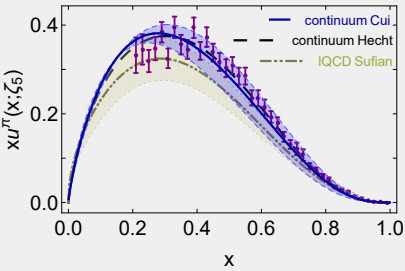

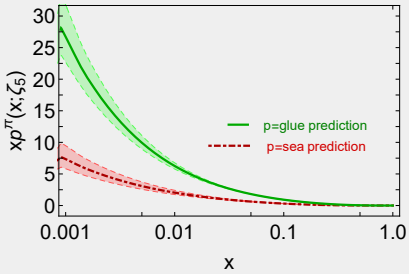

- Within uncertainties, continuum valence distribution (Cui) agrees with continuum in 2001 (Hecht), lattice (Sufian), and rescaled E615 experiment data. Conway et al.. Phys. Rev. D 39 (1989) 92-122. Hecht et al.. Phys. Rev. C 63, 025213 (2001). Aicher et al.. PRL 105, 252003 (2010). Sufian et al.. Phys. Rev. D 99, 074507 (2019). Cui et al., Eur. Phys. J. C 80, 1064 (2020).
- Mellin moments: $\langle 2xu^\pi(x;\zeta_5)\rangle = 0.40(2)$, $\langle x\rangle_g^\pi = 0.45(2)$, $\langle x\rangle_{\rm sea}^\pi = 0.14(2)$.

Phenomenological fits update PDFs by including next-to-leading-logarithm (NLL) resummation effect.

- Double Mellin - does not yield appropriate PDFs at hadron scale.
- Mellin-Fourier - yield PDFs in agreement with $(1-x)^{\beta=2+\gamma}$ behavior at large x .

Barry, Ji, Sato, Melnitchouk, Phys. Rev. Lett. 127 (23) (2021) 232001. Cui et al. Eur. Phys. J. A 58 (2022) 1, 10.

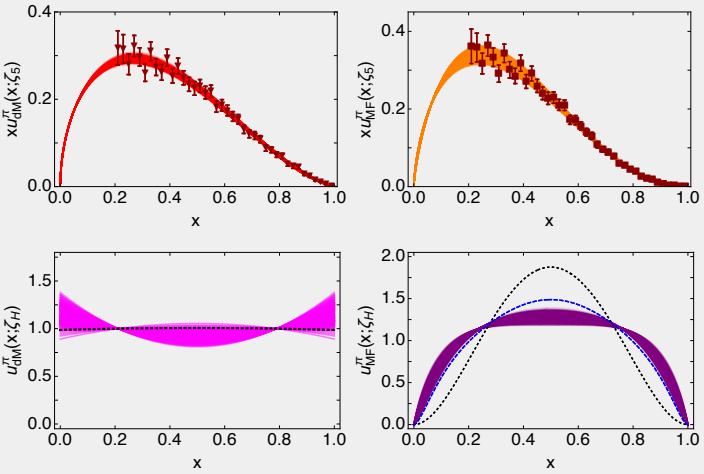

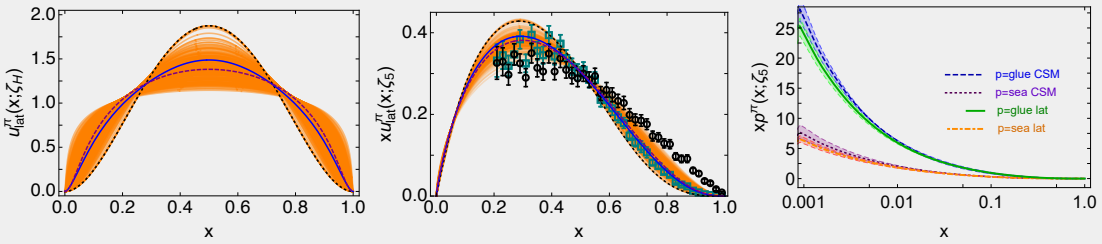

- Exploiting results from numerical simulations of lattice-regularised QCD, parameter-free predictions for pion valence, glue, and sea PDFs are obtained.

  Cui et al. Phys. Rev. D 105 (2022) 9, L091502.

- Supposing only that there is an effective charge which defines an evolution scheme for PDFs that is all-orders exact, strict lower and upper bounds on all Mellin moments of the valence-quark PDFs of pion-like systems are derived.
- Lattice moments fall within the open band. Joó, Karpie, Orginos, Radyushkin, Richards, Sufian, Zafeiropoulos, Phys. Rev. D 100 (2019) 114512. Sufian, Karpie, Egerer, Orginos, Qiu, Richards, Phys. Rev. D 99 (2019) 074507. Alexandrou, Bacchio, Cloet, Constantinou, Hadjiyiannakou, Koutsou, Lauer, Phys. Rev. D 104 (5) (2021) 054504. Cui et al. Phys. Rev. D 105 (2022) 9, L091502.

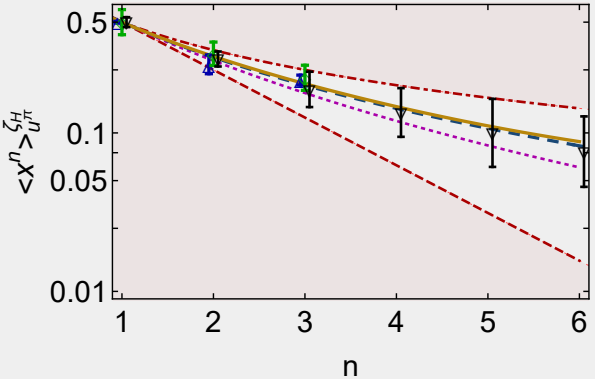

$$\frac{1}{2^n} \leq \langle x^n \rangle^{\zeta}_{u_\pi} \left(\langle 2x \rangle^{\zeta}_{u_\pi} \right)^{-\gamma_0^n/\gamma_0^1} \leq \frac{1}{1+n} \tag{24}$$

- Truncated Hausdorff moment problem $s_k = \int_0^1 x^k f(x)\, dx$ for $k = 0, 1, \ldots m$.
- Necessary and sufficient conditions for the existence of positive $f(x)$: for $m = 2n$,

$$(s_{i+j})_{i,j=0}^{n} \succeq 0\,,$$
$$(s_{i+j+1} - s_{i+j+2})_{i,j=0}^{n-1} \succeq 0\,; \qquad (25)$$

for $m = 2n+1$,

$$(s_{i+j+1})_{i,j=0}^{n} \succeq 0\,,$$
$$(s_{i+j} - s_{i+j+1})_{i,j=0}^{n} \succeq 0\,. \qquad (26)$$

$(s_{i+j})_{i,j=0}^{n}$ represents the Hankel matrix.

- Continuity, unimodality, symmetry of $f(x)$ strengthen the sieve.

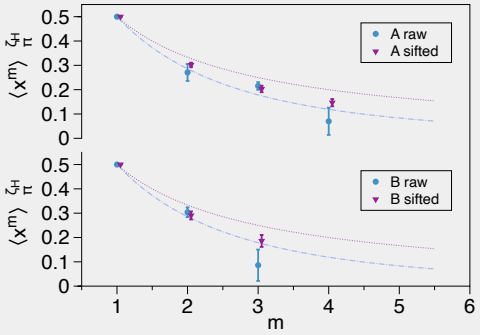

Figure 14: Through an error-inclusive sifting process, we refine three sets of PDF moments from Lattice QCD. This refinement significantly reduces the errors, particularly for high order moments. Wang, Ding, Chang, Phys.Lett.B 851 (2024) 138568

1 Introduction

2 Form factors

3 1D picture of how quarks move within pion

4 A multidimensional view of pion structure

Transverse momentum dependent (TMD) distribution function

- Longitudinal momentum x, transverse momentum k_T.

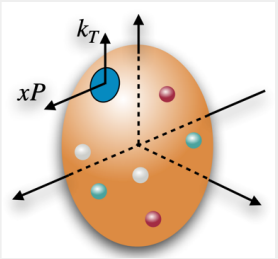

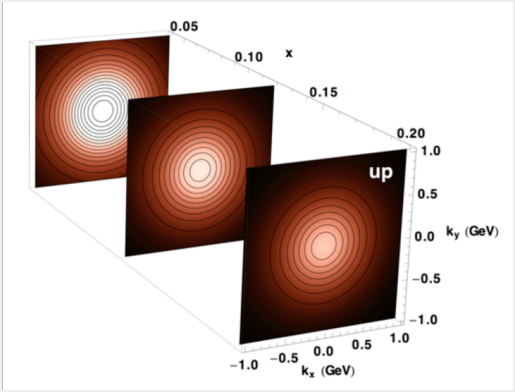

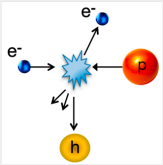

- Semi-inclusive deep inelastic scattering (SIDIS)
- Transverse momentum dependent
- Wilson line, process-dependent, not universal

Gauge-invariant TMD correlation function

Bacchetta, Trento lectures, 2012; Mulders, lectures at the Galileo Galilei Institute (2015).

$$\Phi(x,k_\perp)=\int\frac{d^3r}{8\pi^3}e^{-ixP^+r^-+ik_\perp\cdot r_\perp}\langle P|\bar\psi(0^+,r^-r_\perp)\widetilde{U^\dagger_{(+\infty;r)}}\widetilde{U_{(+\infty;0)}}\psi(0)|P\rangle\,,$$

$$\widetilde{U^\dagger_{(+\infty;r)}}=U^\perp_{(+\infty^-,+\infty_\perp;+\infty^-,0_\perp)}U^-_{(+\infty^-,0_\perp;0^-,0_\perp)}\,,$$

$$\widetilde{U_{(+\infty;0)}}=U^{-\dagger}_{(+\infty^-,r_\perp;r^-,r_\perp)}U^{\perp\dagger}_{(+\infty^-,+\infty_\perp;+\infty^-,r_\perp)}\,. \tag{27}$$

- U^- and $U^{-\dagger}$: resummation of collinear gluons
- $U^\perp$ and $U^{\perp\dagger}$: resummation of soft transversal gluons
- Choosing light-cone gauge, only transversal Wilson lines remain
- Choosing Feyman gauge, only longitudinal Wilson lines remain.

Working at leading twist one may in general rewrite quark + quark correlation function as:

$$\Phi_{q/\pi}(x,\mathbf{k}_\perp) = \tfrac{1}{2}\left[f_{1\pi}^q(x,k_\perp^2) i\gamma\cdot n + h_{1\pi}^{q\perp}(x,k_\perp^2)\tfrac{1}{M}\sigma_{\mu\nu}k_{\perp\mu}n_\nu\right], \tag{28}$$

- $f_{1\pi}^q(x,k_\perp^2)$ is helicity-independent TMD, $h_{1\pi}^{q\perp}(x,k_\perp^2)$ is Boer-Mulders function.
- M is a dynamically generated mass scale that is characteristic of EHM. A sensible choice for pion is $M \approx 4 f_\pi$, where f_π is the pion leptonic decay constant.

It is plain that

$$f_{1\pi}^q(x,k_\perp^2) = \mathrm{tr}\tfrac{1}{2} i\gamma\cdot\bar{n}\Phi_{q/\pi}(x,\mathbf{k}_T), \tag{29a}$$

$$\frac{k_\perp^2}{M^2} h_{1\pi}^{q\perp}(x,k_\perp^2) = \mathrm{tr}\tfrac{1}{2M}\sigma_{\mu\nu}k_{\perp\mu}\bar{n}_\nu\Phi_{q/\pi}(x,\mathbf{k}_T). \tag{29b}$$

- Many studies use $M \to m_\pi$, *i.e.*, the pion mass; however, we judge this to be ill-advised because $m_\pi \to 0$ in the chiral limit whereas f_π does not.

- The helicity-independent TMD, $f_{1\pi}^{q}(x,k_\perp^2)$, is always nonzero; but if the gauge links are omitted, then the Boer-Mulders function vanishes.
- This is the signal that interactions between the spectator of the initial scattering event and the degree-of-freedom struck by the probe are crucial to obtaining $h_{1\pi}^{q\perp}(x,k_\perp^2)\neq 0$.

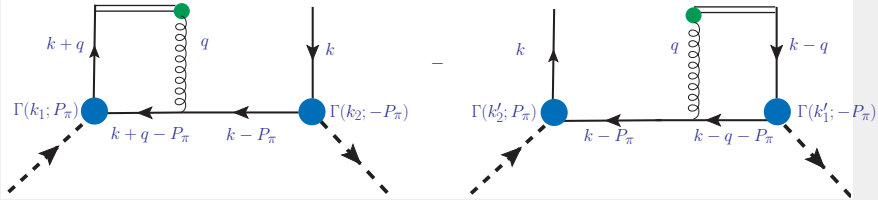

$$h_{1\pi}^{\perp}(x,k_\perp^2)\frac{\vec{k}_{\perp\alpha}}{M} = N_c \mathrm{tr}_{\mathrm{D}} \int \frac{d^4q}{(2\pi)^4}\frac{dk_3 dk_4}{(2\pi)^4}\delta_n^x(k) S(k-P_\pi)\Gamma(-P_\pi)S(k)\sigma_{\alpha+}\frac{[-gn_\mu]}{n\cdot q} \times S(k+q)\Gamma(P_\pi)S(k+q-P_\pi)[-g\gamma_\nu]D_{\mu\nu}(q)\,. \tag{30}$$

The number density asymmetry corresponds to the following difference:

$$f_{q^\uparrow/\pi}(x,\vec{k}_\perp) - f_{q^\downarrow/\pi}(x,\vec{k}_\perp) = -h_{1\pi}^{q\perp}(x,k_\perp^2)\frac{|\vec{k}_\perp|}{M}\sin(\phi_{k_\perp}-\phi_S)\,, \tag{31}$$

where the azimuthal angles are measured between the indicated transverse vector and $\hat{P}$.

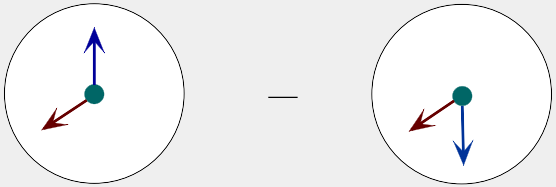

Figure 15: Number density interpretation of the Boer Mulders function. Vertical blue arrows - transverse polarisation of the quark; oblique red vectors - quark transverse momentum vector.

- Exploiting the requirements imposed by positivity of the defining matrix element, one arrives at the pointwise positivity bound:

$$|k_\perp h_{1\pi}^{q\perp}(x,k_\perp^2)/M| \le f_{1\pi}^{q}(x,k_\perp^2)\,. \tag{32}$$

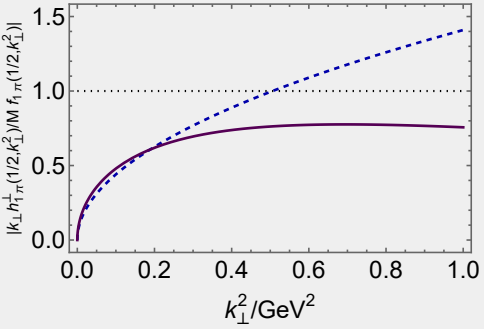

Figure 16: Positivity constraint, Eq. (32): the bound is violated if the curve crosses the horizontal dotted line.
$|k_\perp h_{1\pi}^{\perp \mathrm{MI}}(x=1/2,k_\perp^2)/M f_{1\pi}(x=1/2,k_\perp^2)|$ – dashed blue *cf.*
$|k_\perp h_{1\pi}^{\perp}(x=1/2,k_\perp^2)/M f_{1\pi}(x=1/2,k_\perp^2)|$ solid purple. Cheng, et al, arXiv:2409.11568 [hep-ph].

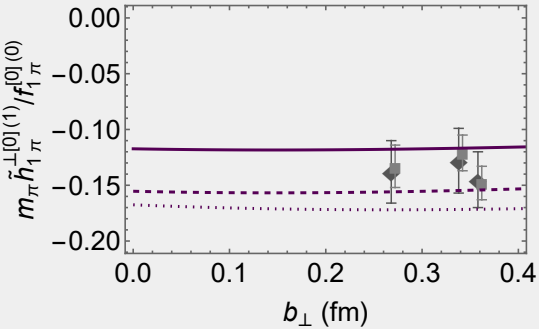

Figure 17: Generalised Boer Mulders shift. Dotted purple curve – hadron scale physical pion mass result; dashed purple curve – hadron scale heavy pion ($m_\pi = 0.518\,\mathrm{GeV}$); and solid purple curve – heavy pion result evolved $\zeta_{\mathcal{H}} \to \zeta_2$. LQCD results, obtained with $m_\pi = 0.518\,\mathrm{GeV}$ at a resolving scale $\zeta = \zeta_2 = 2\,\mathrm{GeV}$.

Connection with electromagnetic form factor (0-th Mellin moment of GPD)

Mezrag, Few Body Syst. 63 (2022) 3, 62.

$$\int_{-1}^{1} dx\, H^q(x,\xi,Q^2) = F_{\rm em}(Q^2)\,, \tag{33}$$

Connection with gravitational form factor (1st Mellin moment of GPD)

$$\int_{-1}^{1} dx\, x\, H^q(x,\xi,Q^2) = A^q(Q^2) + \xi^2 D^q(Q^2)\,, \tag{34}$$

Connection with parton distribution amplitude (in the limit $(\xi, Q^2) \to (1,0)$)

$$H^q(x,1,0) + H^q(-x,1,0) = \varphi\left[(1+x)/2\right]\,, \tag{35}$$

Connection with parton distribution function (forward limit $(\xi, Q^2) \to (0,0)$)

$$H^q(x,0,0) = q(x)\Theta(x) - \bar{q}(-x)\Theta(-x)\,. \tag{36}$$

GPD measurements: (DVCS, TCS, DVMP)

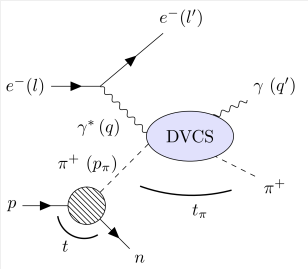

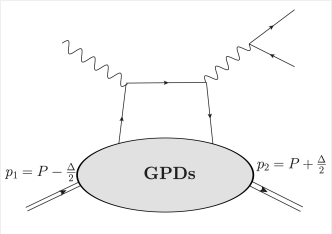

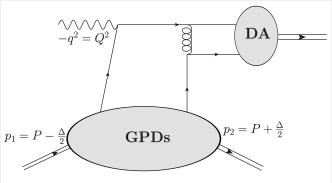

GPD modelling:

- Overlap representation of the light front wave function

  Diehl, Feldmann, Jakob, Kroll, Nucl. Phys. B 596 (2001) 33-65, Nucl.Phys.B 605 (2001) 647-647 (erratum)

- Double Distribution representation

  Mueller, Robaschik, Geyer, Dittes, Horejsi, Fortsch. Phys. 42 (1994) 101-141

$H_\pi^u(x,\xi,-\Delta^2;\zeta_H)$, momentum transfer $\Delta = p' - p$, deviation of the momentum fraction along the lightcone of quark with respect to the average momentum fraction $\xi = -[n\cdot\Delta]/[2n\cdot P]$, average momentum $P = (p+p')/2$, n is light-like vector $n^2 = 0$.

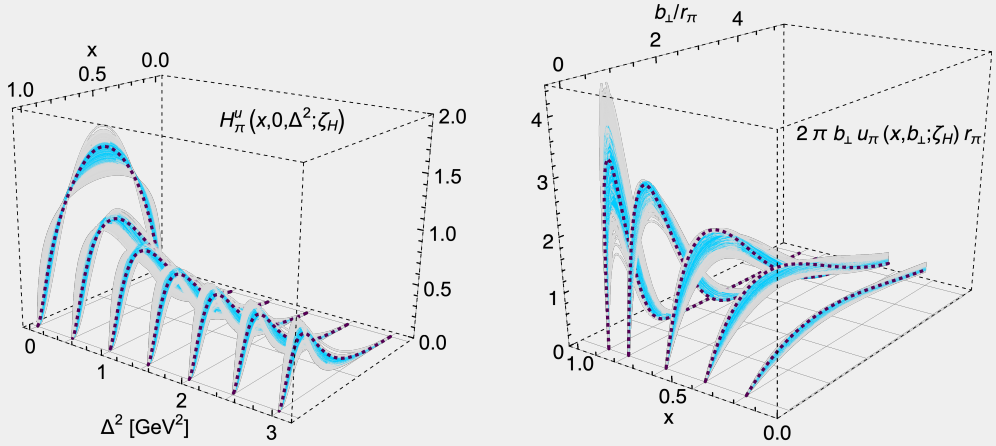

Pion GPD, and GPD in impact parameter space. Xu et al, Chin. Phys. Lett. 40 (2023) 4, 041201.

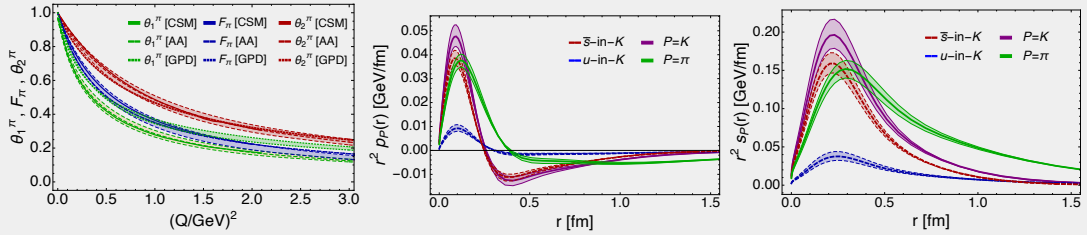

Pion electromagnetic (F_π - blue) and gravitational form factors (θ_1 - green, θ_2 - red), Pressure and shear distributions. Xu et al, Eur. Phys. J. C 84 (2024) 2, 191.

- Pion pressures are large and positive at $r \simeq 0$, with dressed-valence constituents repelling each other. As r increases, the pressure changes sign, transitioning to a region dominated by confinement forces. Zeros occur at $r_c^\pi = 0.39(1)$ fm.
- $r \simeq 0$ pressures therein of roughly 0.1 GeV/fm, so pion core pressures are commensurate with those in neutron stars.
- Deformation forces are maximal in the neighbourhood upon which the pressure changes sign.

Summary

- Form factors: the size, shape and makeup of pion
  Electromagnetic form factor, Two-photon transition form factor, Gravitational form factor
- 1D picture of how quarks move within pion
  Parton distribution amplitude, Parton distribution function (PDF) - future experiments (JLab 22 GeV, COMPASS++/AMBER, EIC, EicC) will provide higher precision measurements
- A multidimensional view of pion structure
  Transverse momentum dependent distribution function (TMD), Generalized parton distribution (GPD)

Outlook

- Nucleon, excited state ...
- TMD, GPD, Fragmentation function ...
  dynamical confinement, critical to extracting TMD from data.


Thank you!